Structural and thermodynamic properties of elemental and bimetallic nanoclusters: an atomic scale study

2000 J. Phys.: Condens. Matter 12 6735

(http://iopscience.iop.org/0953-8984/12/30/306)

J. Phys.: Condens. Matter **12** (2000) 6735–6754. Printed in the UK PII: S0953-8984(00)12365-3

Structural and thermodynamic properties of elemental and bimetallic nanoclusters: an atomic scale study

E E Zhurkin† and M Hou‡§

† St Petersburg State Technical University, Department of Experimental Nuclear Physics, Polytekhnicheskaya 29, 195251 St Petersburg, Russia
‡ Université Libre de Bruxelles, Campus de la Plaine, Physique des Solides Irradiés, CP 234 Boulevard du Triomphe, B-1050 Brussels, Belgium

E-mail: zhurkin@twonet.stu.neva.ru and mhou@ulb.ac.be

Received 6 March 2000, in final form 30 May 2000

Abstract. Structural and thermodynamic properties of elemental and bimetallic nanoclusters are studied at the atomic scale. The modelling is achieved by means of molecular dynamics (MD) and Metropolis Monte Carlo (MC) sampling in the so-called transmutational ensemble. The cohesion model used is based on the second moment approximation of the tight binding model. Copper elemental and Ni_xAl_{1-x} binary alloy clusters are selected as case studies. Particles containing less than $n = 201$ atoms are predicted to be structureless, except when elemental, formed by $n = 13$, 55, 135 and 147 atoms. These so-called magic numbers allow icosahedral geometry. Binding energies are not found to be significantly dependent on morphology, suggesting the coexistence of several isomers. As far as Ni_xAl_{1-x} clusters are concerned, phase stability is systematically studied as a function of x, ranging from 0 to 1 and discussed with reference to the bulk ordered alloy. Except in one special case, and in contrast to elemental clusters, no stable phase at all is found in the smallest clusters ($n < 201$) as they are structureless. In the larger ones, consistently with a recent study with another cohesion model (Campillo J M, Ramos de Dibiaggi S and Caro A 1999 *J. Mater. Res.* **14** 2849), a partition shows up between a core where the bulk stable $L1_2$ and B2 phases are retrieved and a mantle which may be subjected to aluminium segregation. In the range of cluster sizes considered ($n = 13$–10 000), the results suggest that, because of the easy surface segregation, the martensitic metastable phase occurring in bulk Ni–Al systems does not take place in free clusters. The segregation efficiency is found to decrease with increasing cluster size while the relative mantle thickness is size independent. This may be the reason why the martensitic phase only occurs in systems larger than currently investigated.

1. Introduction

The nanometre range has become a typical size in material technologies, and, consequently, the properties of nanostructured materials attract much interest. Nanostructured materials can be produced in various ways and may thus display a variety of properties. Whatever the production method, the common building block is an assembly of atoms whose spatial extension is limited to a few nm^3. Hence, they only contain no more than a few thousand atoms each and atomic clusters containing a few tens of atoms are currently produced. One question is to understand the influence of the cluster assembling method on the properties of the nanostructured materials. Another is to know to what extent the properties of each cluster are retained after assembling. The purpose of the present work is to explore properties of

§ Corresponding author: Marc Hou.

0953-8984/00/306735+20$30.00

free clusters with a view to identifying, in a further step, which ones are retained in cluster assembled elemental and alloy metals. More precisely, we address the question, both for the elemental and the binary alloy cases, of the effect of size on structure, morphology and binding energy. In the case of alloy clusters, the role of segregation in phase stability is extensively discussed.

When isolated clusters are deposited on a surface, their morphologies are found to be dependent on the substrate structure. Metallic clusters deposited on MgO may form truncated octahedra displaying an epitaxial matching with the substrate [1]. On amorphous substrates, they may display decahedral and icosahedral morphologies and these morphologies were reviewed to be influenced by the nature of the amorphous substrate [2]. As far as the structure of small clusters is concerned, whether they are free, supported, embedded or assembled, they can be characterized by diffraction techniques. Unfortunately, morphologies of free clusters in the vapour phase or in a beam are still unknown and it is thus not possible to find a straightforward relation between the free cluster morphologies and as observed in an assembly, after deposition or after embedding. We refer to [3] and [4] for recent direct successful comparisons between atomic scale modelling and experimental observation of deposited and embedded clusters.

Most of the work reported nowadays on metallic clusters concerns elemental ones. Alloy clusters can however be produced and they may display specific properties at the nanoscale. Free clusters are currently modelled at the atomic scale and, owing to the presently available computer capabilities, the smallest ones can be studied fully *ab initio* [5]. The method is however still limited by the size of the system under study. This motivates the use of classical molecular dynamics (MD) and Metropolis Monte Carlo (MC), although two significant drawbacks may be anticipated. One is the possible morphological distortions due to the Jahn–Teller degeneracy and the HOMO–LUMO coupling. The second is the fact that the available classical potential models are semi-empirical and could only be fitted to the bulk properties of macroscopic materials. An interesting range of methods is based on the tight binding approximation, which allows us to evidence quantum contributions to cluster structures, although not all electrons are handled on an equal footing. Tight binding results however do not always cross check with those of full *ab initio* calculations, as exemplified by the case of the Cu_4 molecule. For the latter, the minimal energy configuration at 0 K is predicted as a tetrahedron by the tight binding method in [6] and as a rhombus when handling s and d electrons on an equal footing [7] by the Car–Parinello method [8]. In many cases however, consistency is found, even between classical and *ab initio* calculations. One spectacular example is the correct prediction of the stability of small clusters with a Lennard-Jones and with a Morse pair potential [9]. Capacitance calculations on frozen configurations of nanoclusters obtained classically with the second moment tight binding approximation were performed in two ways. One was to use the macroscopic size dependence of a conducting sphere and the other was to derive it from the density functional theory (DFT). Both approaches gave close to identical results [10].

In what follows, we adopt the classical MD and MC methods and comparisons will be made with more *ab initio* approaches when possible. As case studies, we select copper elemental clusters as copper potentials are extensively assessed and bulk properties are well known. The Ni_xAl_{1-x} system is considered for the study of properties specific to alloy clusters, which are well known to display different bulk phases, depending on x, with no order–disorder transformation below 1000 K [11]. These two cases will allow emphasis of the similarities and differences between characteristics of elemental and bimetallic clusters.

The next section describes the MD and the MC methods used. The third section is devoted to the structural 0 K properties of elemental copper clusters and the fourth section discusses the characteristics of Ni_xAl_{1-x} clusters of similar sizes at all relative concentrations and at

different temperatures. MD is used for modelling elemental clusters while MC sampling is necessary in order to model the binary alloy clusters.

2. The simulation methods

2.1. Initial cluster boxes

As mentioned in the introduction, the morphologies of unsupported clusters are not known and, therefore, no assumption is made about the equilibrium morphology the clusters may have. As much as possible, no assumption either is made on the cluster crystallographic structure and the initial configurations are rather selected in some way which aims at inducing as few as possible final configurations. Different initial conditions will be tried in order to check the convergence toward similar final properties.

As elemental clusters are concerned, generally, the initial configurations are spheres of different radii, cut in an fcc copper lattice. Molten spheres are considered in some cases as well in order to insure that no bias is introduced into the discussion because of an *a priori* initial structure. As far as small clusters are concerned, if they are centred on an atom, cutting a sphere this way always provides odd numbers of atoms. Therefore, in order to obtain even numbers as well, spheres are also centred on a tetragonal site. In order to obtain known magic numbers, atoms selected at random are removed from the sphere surfaces. This way, no icosahedral phase is *a priori* induced. Some ideal truncated octahedra are also considered. They are characterized by {111} regular hexagonal facets limited by {100} perfect square facets. The possible number, N, of atoms in such clusters is well defined and it follows the rule [12]:

$$N(n) = 16n^3 - 33n^2 + 24n - 6 \tag{1}$$

where n is any integer larger than 2. Heating and cooling cycles are applied, as described in section 2.3, in order to identify stable 0 K configurations. As far as alloy clusters are concerned, several phases are known which we thus expect to come out of our simulations. In order to allow a comparison between elemental and alloy clusters, care is taken that the method used to build the initial clusters is similar to that for elemental clusters, starting from ideal $L1_2$ Ni_3Al boxes. In the $L1_2$ phase the Ni atoms sit at the centre of faces of an aluminium simple cubic sublattice, while in the B2 phase the Ni atoms sit at the centre of the aluminium cube. The relation between the lattice parameter lengths in phases B2 and $L1_2$ is: $a_{B2} = a_{L1_2}/2^{1/2}$. No heating–cooling cycle is achieved since the morphology may depend on stoichiometry, *a priori* considered as unknown, and in our model described below, the stoichiometry is temperature dependent. Stoichiometry changes monitored according to the MC method described below induce, among other things, structural phase transitions, which will be discussed in section 4.

2.2. The cohesion models

The cohesion models used in the elemental and alloy cases are similar. They are based on the second moment approximation of the tight binding model [13]. The cohesive energy of the system, projected on one atom, is written as:

$$E_i = \frac{1}{2}\sum_{i\neq j}\varphi_{\alpha\beta}(r_{ij}) + \sqrt{\sum_{i\neq j}\Phi_{\alpha\beta}(r_{ij})} \tag{2}$$

so that the total energy of the system is

$$E_T = \sum_i E_i. \tag{3}$$

In (2), α and β refer to the chemical nature of the interacting atoms. For the functions $\varphi_{\alpha\beta}$ and $\Phi_{\alpha\beta}$, we adopt the functional dependences suggested in [14]. These functions are formed by cubic spline segments limited by cut-offs bringing the resulting forces to a range slightly beyond the third neighbour distance. Several fittings of the parameters involved in these functions are suggested in the literature. For the elemental copper clusters, we selected those suggested in [14] while for the Ni–Al system, those suggested in [15] were preferred since they lead to a reasonable prediction of macroscopic properties of the $L1_2$ Ni_3Al phase. Further assessment for other stoichiometries comes out the MC simulations presented in section 4 for bulk materials. The same potential form was successfully applied to study interface properties of Ni_3Al [16, 17] as well as order–disorder phase transitions in bulk Cu_3Au [14, 17], at various grain boundaries [18] as well as at surfaces [19].

2.3. The molecular dynamics model

MD and MC are two different ways of phase space sampling at finite non-zero temperature and, therefore, both techniques lead to the same evaluation of macroscopic observables. Therefore, the selection of one or another technique is driven by efficiency. In many circumstances, average thermodynamic quantities may be obtained by MD within a reasonable accuracy with a limited number of iterations. Moreover, efficient quenching algorithms allow prediction of 0 K equilibrium configurations with minor computing efforts. In contrast, MD is totally inefficient when infrequent events are involved like diffusion jumps, segregation and, to some extent, phase transformations. In such circumstances, the Metropolis MC with suitable sampling algorithms is more efficient. Sampling does not need to be achieved along physical paths. The MD model used is described in this section and the MC model in the next one, the former being used for elemental Cu clusters and the latter for the Ni_xAl_{1-x} clusters with all values of x between 0 and 1. Particular care was taken in the MD simulations to obtain an efficient energy minimization and thus reasonably probable isomers when several distinct ones are possible, which is the most general case. The results served as a reference for the MC simulations of alloy clusters. Since the details of the evolution of the initial clusters to thermodynamic equilibrium are not the subject of this work, the dynamic coupling between the ionic and the electronic systems is discarded and we limit ourselves to solving the Newton equations of motion stepwise in time for the ions only. These are however modified by the introduction of a velocity dependent force in view of thermalizing the clusters. Initially, all atoms are randomly displaced from their geometrical sites. The cluster is then brought to thermal equilibrium according to the equations of motion:

$$\boldsymbol{F}_i = -\nabla_i E - m_i \alpha \frac{T_i(t) - T_f}{T_i(t) + \varepsilon} \boldsymbol{v}_i \tag{4}$$

where $T_i(t)$ is the current instantaneous temperature of atom i, $\boldsymbol{v}_i$ its velocity, α is the inverse characteristic heating time taken for convenience to be of the order of 1 ps and ε is a small non-zero constant used to avoid singularities when the instantaneous temperature of an atom tends to zero. This way, most of the thermal excitation is included in the vibrational modes and the angular momentum induced by the velocity dependent term in equation (4) turns out to be negligibly small. In the absence of boundary conditions, the latter keeps constant, within the accuracy of numerical round-offs in the force calculations.

The elemental clusters are heated up to 600 K or 750 K depending upon their size, according to equation (4), and they undergo a free evolution for a period of time at least 100 ps long (200 ps for the largest clusters considered). No higher temperature is used in order to prevent evaporation or dissociation. The clusters are then smoothly cooled down to 0 K by velocity re-scaling at a rate of about 5 K ps^{-1}. A further free evolution of a few ps is then allowed in

order to insure that an equilibrium configuration is reached. The procedure is repeated by spot with different initial temperatures, some above the melting temperature, in order to insure that the same final configuration is found.

The final configurations were examined by visual inspection, pair correlation functions and central distance distributions. The latter is preferred in cases where surface disorder and relaxation may hide the core structure characteristics in the pair correlation function. Otherwise, the information carried by both functions is similar.

2.4. The Metropolis Monte Carlo model

The Metropolis MC method is widely used for studying the equilibrium properties of liquids and solids. The general algorithm is well described, e.g. in [20]. Here we employ the MC method in the so-called 'modified grand-canonical ensemble with transmutations' ($\Delta\mu NPT$) [21]. In this approach the total number of the particles ($N = N_{Al} + N_{Ni}$), temperature (T), pressure (P) and chemical potential difference† ($\Delta\mu = \mu_{Al} - \mu_{Ni}$) are fixed. The partial number of each kind of atom (N_{Al}, N_{Ni}) may be changed. The method includes three types of trial:

(i) *Random displacement of each atom of the model box from its current position.* The magnitude of this displacement is dynamically adjusted in order to optimize convergence. It is of the order of three thousandths of an ångström. The decision on acceptance of a new configuration is based on the relation between probabilities according to the standard Metropolis method:

$$P_{new}/P_{old} = \exp\{-\Delta U/kT\} \tag{5}$$

where kT is the Boltzmann factor and ΔU is the potential energy difference. If the ratio P_{new}/P_{old} is larger than unity, the new configuration is accepted anyway. Otherwise, it is accepted with the probability P_{new}/P_{old}.

(ii) *The chemical identity of an atom selected at random is changed with relative probability*

$$P_{new}/P_{old} = \exp\{-(\Delta U - \Delta\mu)/kT\}. \tag{6}$$

(iii) *The site of this atom is exchanged with another one selected at random in the box.* The decision on acceptance in this case is based on relation (5).

One set of these three trials applied on all atoms in the system is called a 'macrostep'. After all atoms in the box have undergone several macrosteps, the lattice parameter of one of randomly selected box direction [001], [010] or [100] is changed at random. We found it efficient to use trials for huge volume changes by allowing changes in the lattice parameters up to 1 Å, i.e. up to 25% of the $L1_2$ lattice parameter value. The relative probability of this acceptance is:

$$P_{new}/P_{old} = \exp\{-(\Delta U + P\Delta V - NkT\Delta \ln V)/kT\} \tag{7}$$

where V is the volume of the box.

This acceptance test insures a convergence of the pressure P to a given value, taken as zero in this work. It also allows for orthogonal, though non-isotropic, changes in the box shape. This way, the transitions between $L1_2$, $L1_0$ and B2 phases are possible. This transformation indeed requires different lattice constant length changes in different directions. The achievement of the thermodynamic equilibrium is judged by controlling the evolution of instantaneous quantities such as cohesive energy, partial concentrations of atomic species and pressure. Typically, the equilibrium lattice constant is reached after several hundred macrosteps. In contrast, up to one million macro MC steps may be necessary to reach local equilibrium at the atomic scale.

† The definition of the chemical potential is very standard and may be found, for instance, in [22].

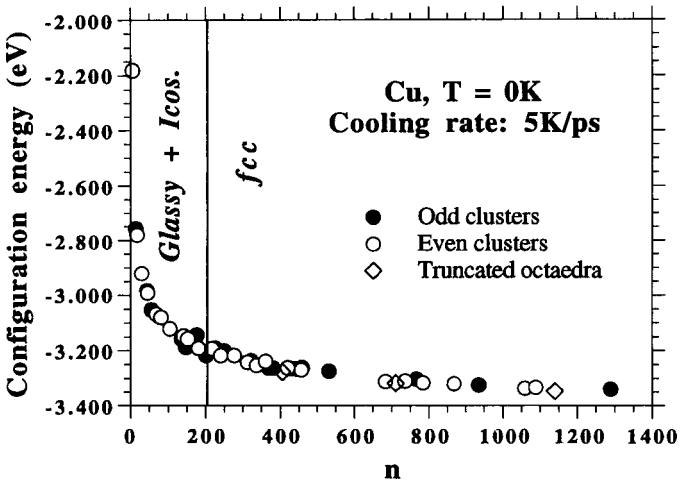

Figure 1. The copper cluster configuration energy as a function of n, the number of atoms forming the clusters. The transition line at $n = 201$ is given. Clusters are either glassy or icosahedral when $n < 201$ and fcc otherwise.

3. Elemental clusters

Figure 1 shows the cluster size dependence of the configuration energy measured at 0 K (the configuration energy is just the negative of the binding energy). Similar results obtained with a mean field model are given in [23], which focus on free cluster morphologies. Clusters are considered with more than $n = 1415$ atoms, which is the upper limit in figure 1. The results differ by no more than 1% from ours. They are thus not very potential sensitive, indicating that both the study in [23] and the present one are complementary. For $n > 1400$, the binding energy is found in [23] to be linearly dependent on $n^{-1/3}$. The same dependence is easily deduced from figure 1 for all n-values larger than 4. The distinction is made between clusters having even and odd numbers of atoms. The results for some truncated octahedral clusters are shown as well. A universal monotonic decrease of the configuration energy with the cluster size is found, which is not significantly dependent either on the parity of the number of atoms or on the cluster morphology. The highest measured configuration energy is -2.18 eV per atom for $n = 4$ and the lowest is -3.35 eV for $n = 1280$, which is still significantly above the bulk value of -3.5 eV. The divergence from the tight binding estimate in [6] is significant for $n = 4$ (the present energy value is close to a factor of 2 lower) but becomes less serious as n increases. It is close to 10% for $n = 13$ and becomes insignificant for $n = 100$. This gives an idea of the magnitude of the classical approximation. It should be noticed however that other parametrizations of the second moment classical tight binding potential are possible which were not tried here. More insight about the cluster structures found comes from figure 2 where central distance distributions are given. The distributions for $n = 147$ and $n = 201$ display well defined structures. In contrast, the others are characteristic of glassy systems. MD already predicted such a disordering for the Al_{43} [15] molecule, which can be expected to be rather similar to our results in figure 2(a). Photoelectron spectroscopy measurements suggested evidence for geometrical packing in aluminium, only for $n > 100$ [24]. The distribution in figure 2(b) ($n = 147$) is typical of a three shell arrangement in the icosahedral phase. The closest shell contains 12 atoms, the second 42 and the third 88. One atom sits at the centre. It was indeed found that, for $n < 201$, order only occurs when the

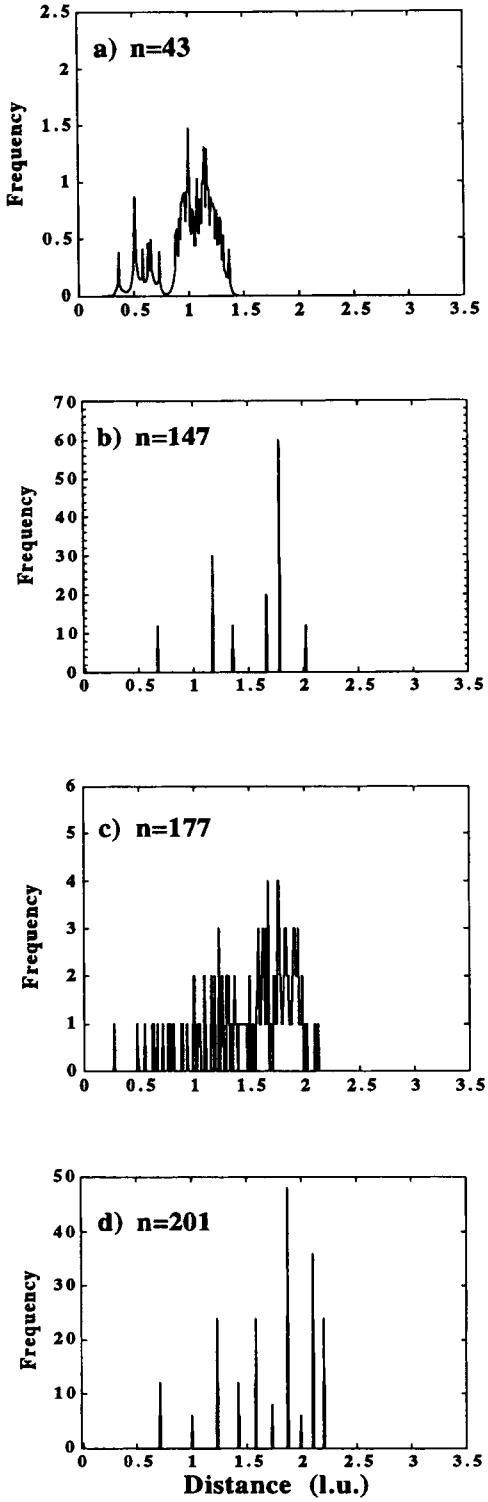

Figure 2. The central distance distribution functions for the Cu clusters containing (a) 43, (b) 147, (c) 177 and (d) 201 atoms.

number of atoms fits closed shell icosahedra and not otherwise. The only exception found is for $n = 135$ which corresponds to the three shell icosahedron with the 12 vortices of the outer shell vacant. In contrast, the distribution in figure 2(d) ($n = 201$) is that of an fcc ordering. According to equation (1), this is the smallest possible ideal truncated octahedron, which is the faceted morphology minimizing the surface to volume ratio. Whatever the n-value, all larger clusters found were fcc, displaying various morphologies. The difference of 0 K configuration energies between the icosahedral phase and the fcc octahedra was measured for $n = 13$ and $n = 55$. The fcc clusters are more weakly bound and the difference is 0.1 eV per atom for $n = 13$. It is more significant for $n = 55$, namely, 0.4 eV per atom. Small differences for $n = 13$ are qualitatively consistent with the DFT estimates including relativistic effects for gold [25]. It is worth mentioning that the fcc structure with cuboctahedral morphology was predicted to be more stable than icosahedral for Pd_{13} and Pt_{13} by means of DFT calculations [26]. On this basis, it may not be excluded that, owing to vibrational entropy at finite non-zero temperature, both isomers coexist. Consistently with [23], we found however that the Cu_{13}, Cu_{55} and Cu_{147} icosahedral molecules predicted in the present work are stable at temperatures as high as 600 K. Although this finding is consistent with experimental observations as well, it represents no proof that different isomers cannot exist as the stability is only checked on time scales reachable by MD, that is, typically, of the order of the nanosecond.

Others [27, 28] have already predicted the size dependence of the structural phase. [27] shows evidence for an fcc to hcp transition in Co_n clusters at a diameter of 40 nm while [28] gives evidence for preferential icosahedral small copper clusters and fcc larger ones. This was supported by electron diffraction by a cluster beam and also by MD calculations. In these calculations, the authors found stable icosahedra with a diameter as large as 3.5 nm and they suggest this size to be a limit for the icosahedron/fcc transition. This is not what is found here since the present modelling predicts the occurrence of the fcc phase for $n = 201$, which corresponds to a diameter of about 1.7 nm, hence, significantly smaller. Diffraction measurements combined with transmission electron microscopy observation of clusters after deposition show, according to [28] that 3.5 nm should be considered as an upper limit. On the other hand, the way the clusters were prepared in the present work is not in contradiction with the possibility of larger icosahedral clusters than $n = 147$ (1.45 nm diameter). Figure 1 as well as the small differences in fcc and icosahedral configuration energies suggest the coexistence of several isomers of the same size. The relative populations may be temperature dependent and their prediction will require careful free energy calculations that are beyond the scope of the present work.

4. Alloy clusters

4.1. Bulk Ni–Al alloy

The equilibrium composition and structure of bulk $Ni_{1-x}Al_x$ alloy can be determined and studied at constant N, P, T and $\Delta\mu = \mu_{Al} - \mu_{Ni}$ with x ranging from 0 to 1. This was done for the whole range of $\Delta\mu$-values fixing x, the relative Al concentration, from 0 (pure Ni) to 1 (pure Al). In what follows, the pressure is imposed to be zero. Before studying the isolated cluster properties, we focus on the case of bulk $Ni_{1-x}Al_x$. The equilibrium relative concentration of Al against $\Delta\mu$ is presented in figure 3 for two different temperatures and similar temperatures dependencies are found from $T = 40$ K to $T = 500$ K. The initial configuration of the simulated box was $L1_2$ and evolves, by phase space sampling, toward the equilibrium structure and composition as governed by the constant N, P, T and $\Delta\mu$ values.

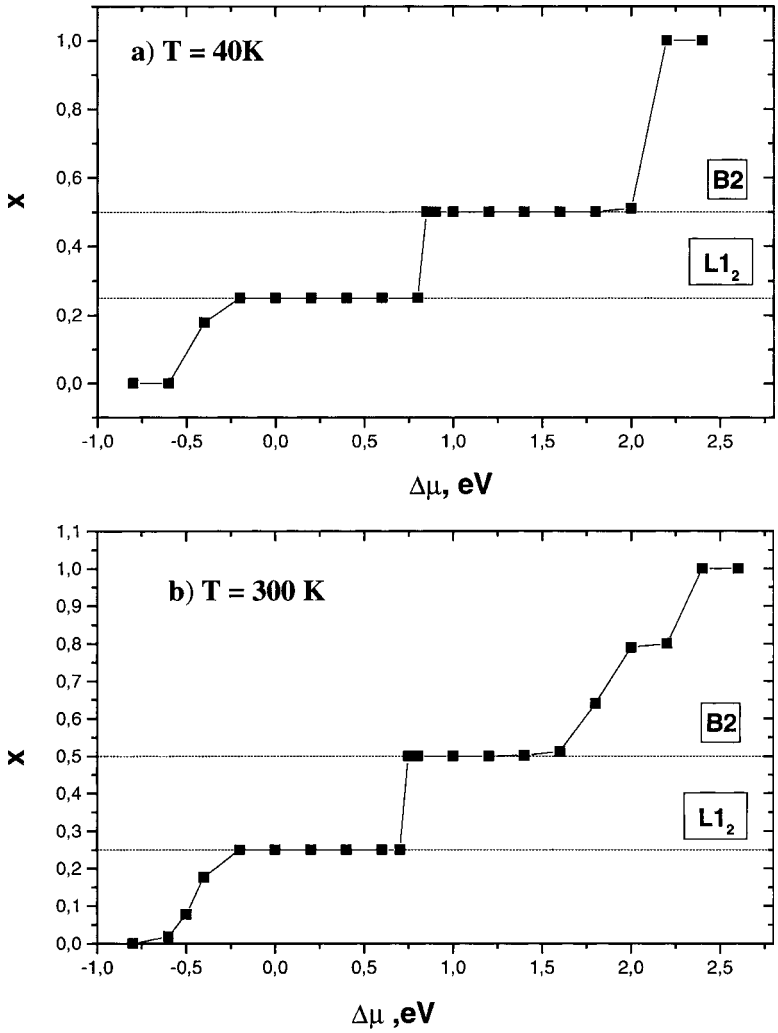

Figure 3. Calculated equilibrium Al concentration as a function of the chemical potential difference, $\Delta\mu$, at zero pressure and temperatures of (a) 40 K and (b) 300 K. The horizontal lines refer to the x-values corresponding to the stable $L1_2$ and B2 phases.

These curves provide information about stable bulk phases. The plateaux at the composition of 25% and 50% are clearly seen. They correspond to two stable phases. Both visual inspection and pair correlation functions allow us to conclude that these plateaux correspond to the ordered $L1_2$ phase of Ni_3Al and the ordered B2 phase of NiAl. Consistently with the experimental phase diagram [29] they were found to take place on the whole considered temperature range investigated in this work. The pair correlation functions for the equilibrium Ni_3Al structure at 300 K are shown in figure 4(a). The peak positions are exactly those expected in the $L1_2$ phase. Only Ni atoms have first neighbours and, accordingly, the first neighbour peaks display no Al contribution. At the second neighbour distance, there is an aluminium contribution and the nickel contribution is three times larger. Only Ni has third neighbours and there is thus no Al contribution to the third neighbour peak, and so forth. The peak widths as displayed cannot

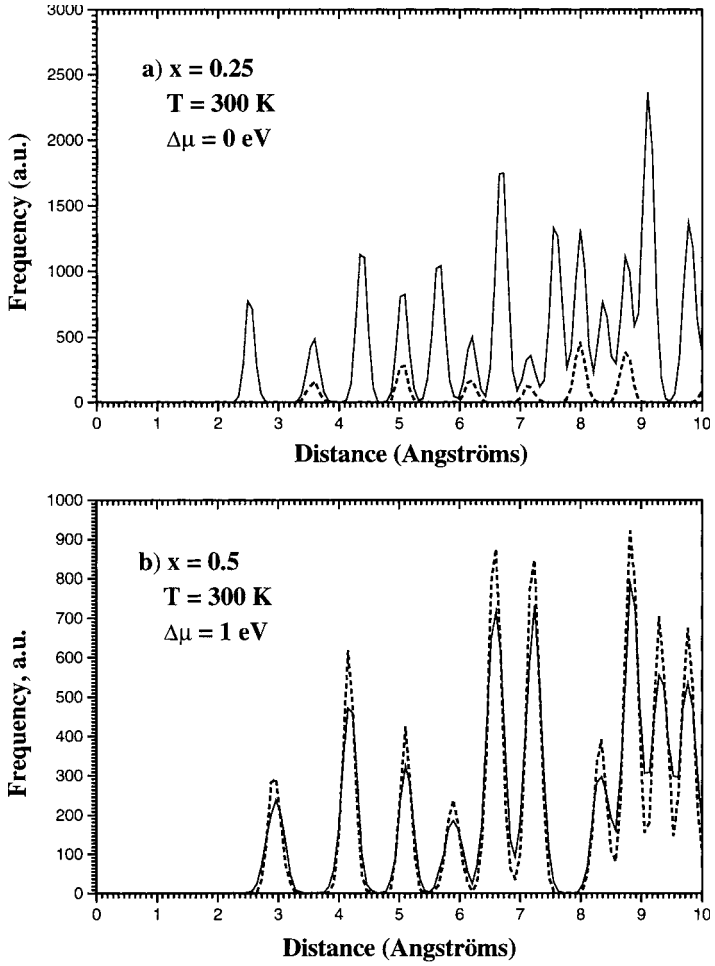

Figure 4. Pair correlation functions for bulk $Ni_{1-x}Al_x$ stable phases. (a) Ni (solid line) and Al (dashed line) pair correlation functions for the bulk Ni_3Al at $T = 300$ K and Al concentration of 25%. (b) Ni (solid line) and Al (dashed line) pair correlation functions for the bulk NiAl at $T = 300$ K and Al concentration of 50%. The channel width is 0.1 Å.

be analysed in detail because they result from the convolution of the histogram channel width and the thermal broadening. The channel width was selected to insure statistical significance of intensities within limited computer times. Some background resulting from distant peaks overlap is due to thermal disorder. No diffusion is observed, which would produce background between small distance peaks as well. Similarly, the radial pair correlation function is displayed in figure 4(b) for the NiAl equilibrium structure. The peak positions are those of the perfect B2 structures. In contrast with the case of the $L1_2$ ordering, nickel and aluminium contribute to each peak on an equal footing and they are found to match exactly those of the ideal B2 structure. Again, thermal disorder contributes to peak broadening, leading to peak overlaps at large separation distances and some subsequent background.

The data presented above are in agreement with those of [30], which were obtained at higher temperature (1000 K), using a similar MC technique, but another potential. The potential used in [30] was based on the embedded atom model (EAM). This shows that the phase stability

Table 1. The $L1_0$ lattice parameters c and a (in ångströms) of $Ni_{1-x}Al_x$ bulk alloys at the different values of x.

Al concentration	Calculated values ($T = 0$ K)			Experiment (room temp.)		
x	a	c	a/c	a	c	a/c
0.250	3.567	3.567	1.0	3.566	3.566	1.0
0.306	3.64	3.48	1.05			
0.35	3.91	3.16	1.237	3.7	3.16	1.19
0.370	3.91	3.17	1.23	3.83	3.18	1.2
0.370[a]	3.93[a]	3.18[a]	1.24[a]			
0.417	3.98	3.13	1.27			
0.5	4.05	3.08	1.31	4.08	2.89	1.4
0.5[a]	4.17[a]	2.96[a]	1.41[a]			

[a] Calculations at $T = 300$ K.

is not very sensitive on the detail of the potential function. This question is further discussed in the next section.

The $Ni_{1-x}Al_x$ phase diagram [29] predicts the possible occurrence of the $L1_0$ martensitic phase for the x-range between 0.35 and 0.37 at 300 K, consistently with recent experimental observations [29]. At the same time, in our simulations, no $L1_0$ stable phase is predicted, even at very low temperature. This is consistent with the modelling results in [30] obtained at higher temperature (1000 K). This narrow range of x-values (0.35–0.37) fits the gap in figure 3 between the two plateaux allocated to the $L1_2$ and B2 phases. This indicates that the simulation result in figure 3 does not allow us to evidence the $L1_0$ phase, which is metastable. The metastable structures for x between 0.25 and 0.5 may however be evidenced at the atomic scale and the equilibrium structure can be determined for each $Ni_{1-x}Al_x$ by fixing x. One efficient method therefore is the Rahman–Parinello MD technique [31, 32]. It allows the dynamic macroscopic lattice transformation to the equilibrium lattice structure at the given value of x. We performed such simulations at zero pressure and 0 K for x ranging between 0.25 and 0.5. The initial structure was selected as a perfect $L1_0$ with $x = 0.5$ and then the excess of Ni was introduced by replacing some Al atoms by Ni isotropically distributed in the volume of the simulated box. Results are presented in table 1. At $x = 0.5$ the structure is close to B2 while for $x < 0.5$ the ratio c/a is close to the tetragonal $L1_0$ structure. The c/a ratio, as well as the a and c parameter values are in agreement with the experimental phase diagram data [11, 29]. The small differences (no more than 5%) may result from the fact that the calculations are performed at 0 K while the experimental data are obtained at room or other non-zero temperature. It should be noticed that at room temperature, these x-values bring the system close to the $L1_0$/B2 first order phase transition. Since first order transitions are characterized by a divergence of thermodynamic fluctuations, size effects in the simulation box need to be carefully taken into consideration. A box with more than 50 000 atoms was necessary in order to avoid them at $T = 300$ K and $x = 0.37$. With this precaution, table 1 shows that the Ni–Al alloy properties are reasonably reproduced with the cohesion model presently used.

4.2. Bimetallic clusters

We now turn to free nanoparticles. A first study of $Ni_{1-x}Al_x$ clusters containing 959 atoms [33] was made using a similar MC algorithm as ours but a different model potential, namely the EAM potential suggested in [30]. In this work, at a temperature of 500 K, no clear evidence

was found for stable phases when the cluster is considered as a whole. It was also shown that the cluster composition is non-uniform: there is a region called 'the core' in which the structure is ordered $L1_2$ or B2 (as in the bulk case) surrounded by a disordered region called 'the mantle' entirely responsible for the deviation from ideal stoichiometry. Generally, no sharp boundary occurs between the core and the mantle, and the core radius ranges from about 60 to 70% of the total cluster radius. An $L1_0$ metastable phase was however found in [33] in a rather wide range of relative Al concentration, namely between 37 and 51 at.%. This appeared as intermediate between $L1_2$ and B2.

In order to cross check our results with those in [33] we generate a similar Ni–Al spherical nanocluster of 2.8 nm diameter, containing 959 atoms. We start with an initial perfect $L1_2$ configuration. Then we repeat the same series of calculations as for the bulk material, except that no periodic boundary conditions are applied. As in [33], the temperature used is 500 K. Figure 5(a) shows a comparison with the results in [33] as well as with those obtained in the previous section. We also display the relative concentration dependence on the chemical potential difference in the central area of the cluster. At this point, several features can be emphasized. First, there is a good overall agreement between the prediction we obtain using a TB potential and the results in [33] using an EAM potential. This means that the cluster properties are not critically potential dependent. The influence of the potential model however merits a more detailed study which is planned for future work. Second, the present results confirm that the dependence of x on $\Delta\mu$ for the bulk sample and the nano-particle, taken as a whole, are quite different and no evidence for stable phases comes out from dependence for the cluster. Indeed, the composition monotonically increases with the chemical potential difference. Third, when the relation between x and $\Delta\mu$ is examined in the core of the cluster only, it closely resembles that found for the bulk in the previous section. This is confirmed by a visual inspection of the cluster at various relative Al concentrations. For instance, when the Al concentration is around 25% or 50%, the cluster displays a highly ordered core surrounded by a chemically disordered mantle in which Al segregates. The $\Delta\mu$ dependence of composition in the core region as shown in figure 5(a) is pretty similar to that in the bulk and clearly indicates two stable phases in the core region: $L1_2$ and B2. Visualization results are fully confirmed by the inspection of the pair distribution functions of Al and Ni atoms represented for the core and mantle regions in figure 6(a) and (b), respectively. When the Al concentration in the core is close to 25%, the positions of the peaks in the core region are the same as those in the perfect $L1_2$ structure. In the mantle region the positions of the Al and Ni peaks just occupy the positions of the fcc structure and no other spatial order is found. Such a morphology where a core can be distinguished from a mantle is found in the $\Delta\mu$ range from -0.2 eV to 0.6 eV, that is, in the range where $L1_2$ stable phase can be found. In this range the overall Al concentration values are between 0.25 and 0.35 at temperatures up to 300 K, as shown in figure 5, while they are almost temperature independent below 300 K (figure 5(c)). Segregation is significantly enhanced at higher temperatures as indicated by the results at 500 K (figure 5). The maximum value of segregation in the $L1_2$ phase at 300 K is reached at $\Delta\mu = 0.6$ eV and corresponds to 34% of Al in the whole cluster which partitions between 25% and 40% in the core and mantle, respectively.

Figure 7 shows the pair correlation function in the core and in the mantle of the cluster when the Al concentration is around 50%. The temperature is 300 K. It clearly comes out from figure 7 that the core has a structure close to the B2 ordered phase, while in the mantle, the Al and Ni atoms occupy the bcc lattice sites at random. Such a partition between the core and the mantle appears for $\Delta\mu$ ranging from 0.8 to 1.6 eV, which corresponds to overall Al concentration ranging from 0.5 to 0.65. Again, no significant temperature dependence of segregation is found below 300 K. The maximum value of segregation at 300 K is reached at

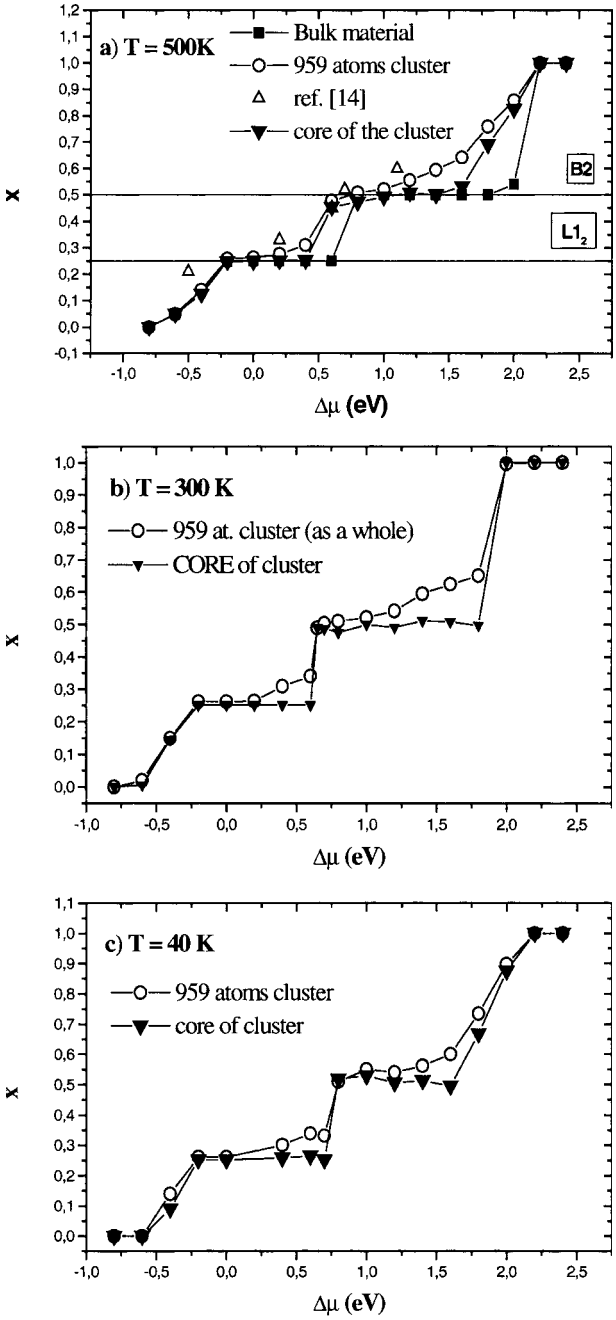

Figure 5. Calculated equilibrium concentration of Al, x, as a function of the chemical potential difference, $\Delta\mu$, for at zero pressure. (a) 500 K, (b) 300 K, (c) 40 K.

$\Delta\mu = 1.6$ eV and corresponds to 61% of Al in the whole cluster and 50% and 66% in the core and mantle, respectively. The radius of the core region is about 60% of whole cluster radius for both the $L1_2$ and the B2 phases.

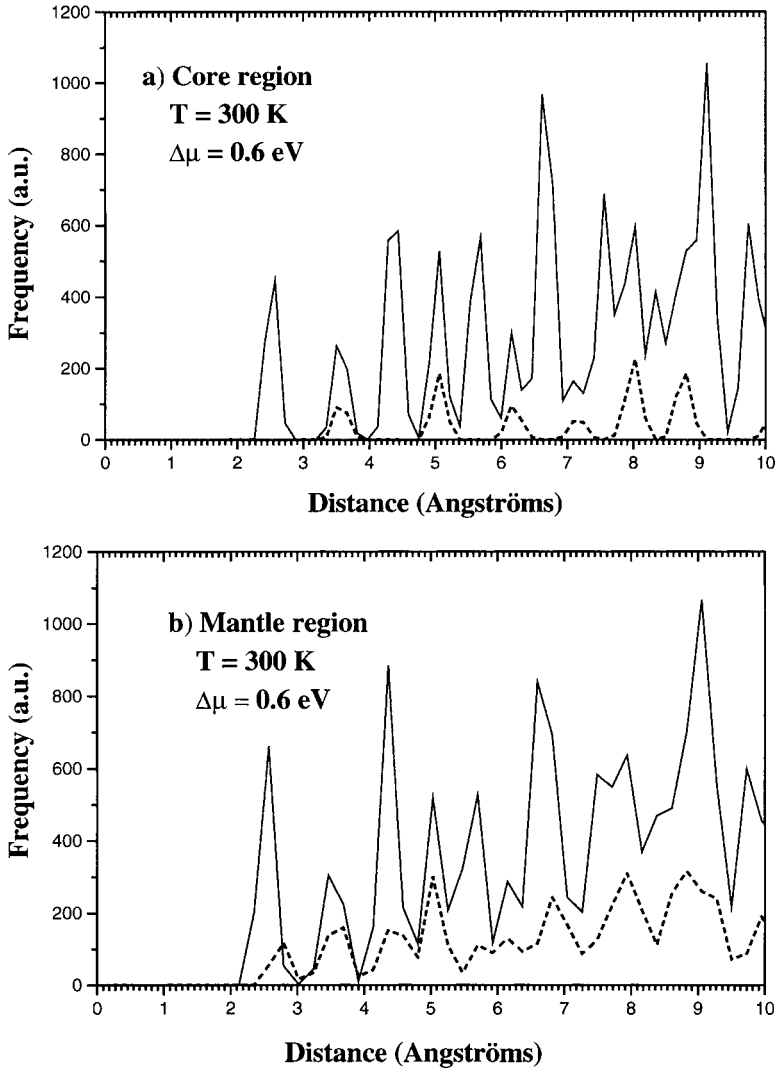

Figure 6. Pair correlation functions for bulk $Ni_{1-x}Al_x$ cluster containing 959 atoms, at $T = 300$ K, with $x = 0.3$: (a) core region, channel width of 0.2 Å, (b) mantle region (channel width of 0.3 Å).

These results are consistent with those in [33] except for the $L1_0$ metastable phase, which is not detected in our simulations. Instead, the excess aluminium segregates at the surface, leaving the core in its stable phase. The reason for this divergence still needs to be identified.

As a next step we investigate the size dependence of cluster properties. Therefore, we generate the set of clusters containing from $n = 13$ to $n = 11\,848$ atoms, hence covering three orders of magnitude. The clusters with $n > 200$ all have similar properties as described above for $n = 959$, while the smaller ones have a different structure. Figure 8 shows the Al concentration as a function of $\Delta\mu$ for the clusters containing 13, 55, 147 and 201 atoms at room temperature and at zero pressure. One can see that the 201-atom cluster displays the same features as discussed above. The same partition between the ordered stoichiometric core

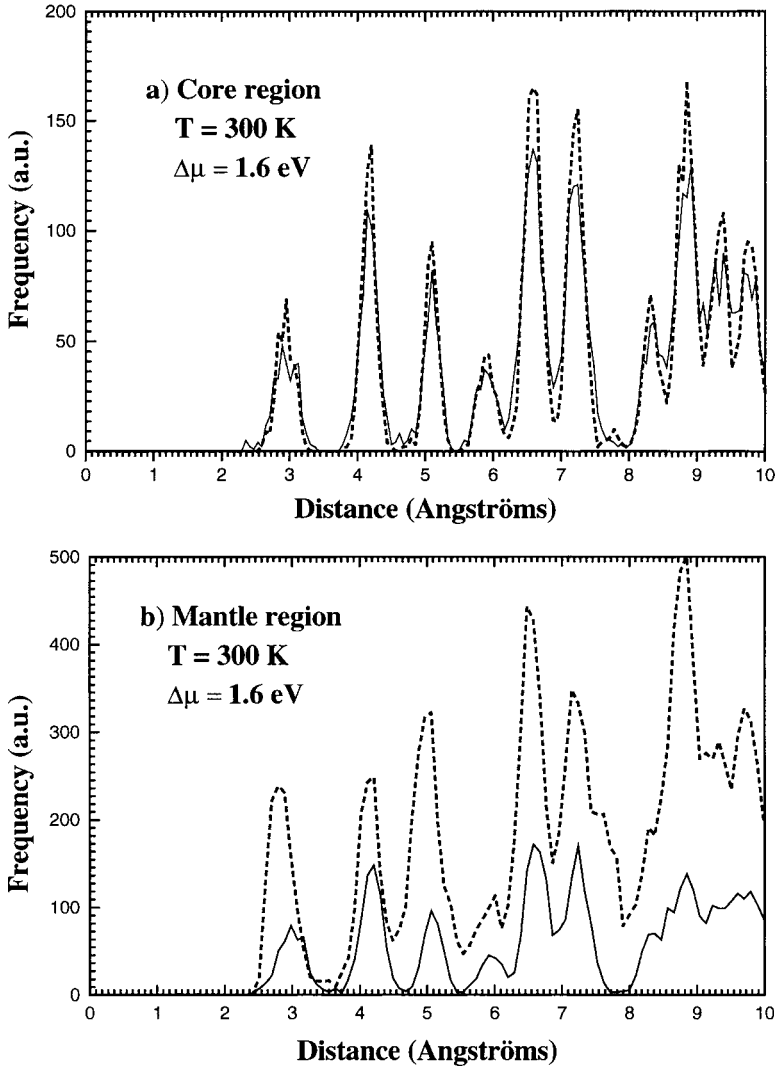

Figure 7. The same as figure 6, with $x = 0.6$. The channel widths are both 0.1 Å.

and a segregated mantle is found. When $n < 201$, clusters display no stable phases, even when $n = 55$, 135 and 147, for which elemental clusters are found to be icosahedral. The 13-atom cluster however displays a stable configuration with one central Ni atom surrounded by 12 Al atoms. An overall dependence of the segregation effect on the cluster size for $n > 201$ is given in figure 9. The chemical potential difference is $\Delta\mu = 0.6$ eV. The Al concentrations in the whole cluster, in the core and in the mantle are distinguished. The segregation effect is found to decrease with increasing cluster size. In all the considered clusters, the structure of the core is the ordered $L1_2$, while the excess of Al segregates at the surface. The structure of the mantle is geometrically ordered fcc, without chemical order. Figure 10(a) shows the Al concentration among the first neighbours of the Ni atoms as a function of the radial distance relative to the cluster radius. In the perfect $L1_2$ order, this

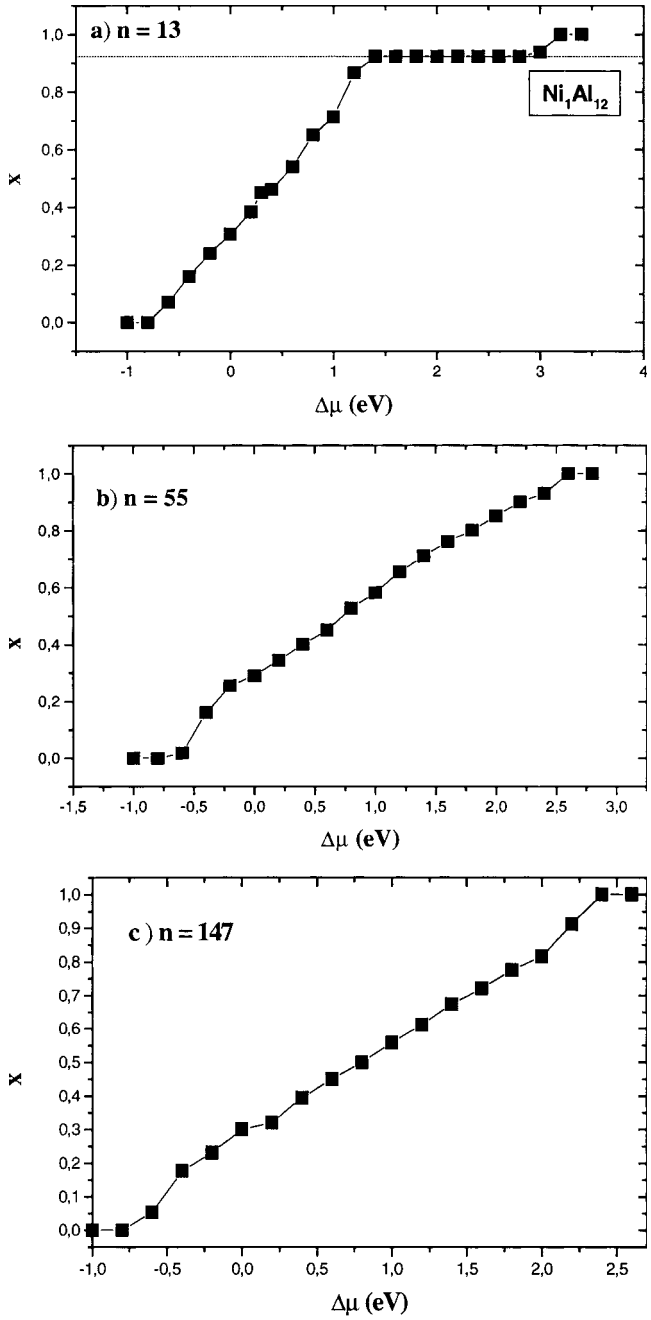

Figure 8. Calculated equilibrium concentration of Al, x, as a function of the chemical potential differences at zero pressure, for nanoparticles of different sizes containing (a) 13, (b) 55, (c) 147 and (d) 201 atoms. In figure 8(d), the results are given for both the whole cluster and for its core only. The x-values corresponding to the stable phases are indicated.

relative concentration is exactly $1/3$. All the clusters are considered at room temperature and the same value of the chemical potential difference is used. One can see from figure 10(a) that

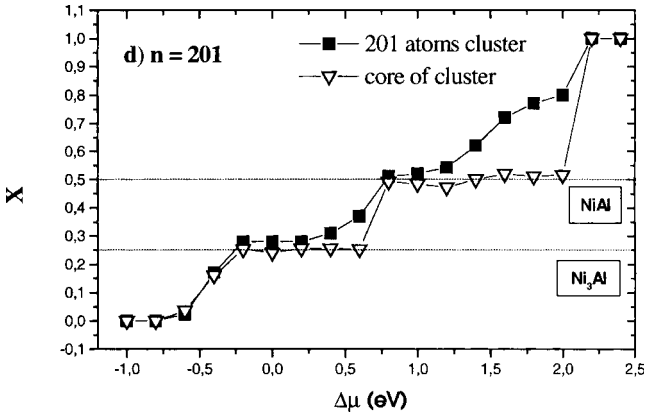

Figure 8. (Continued)

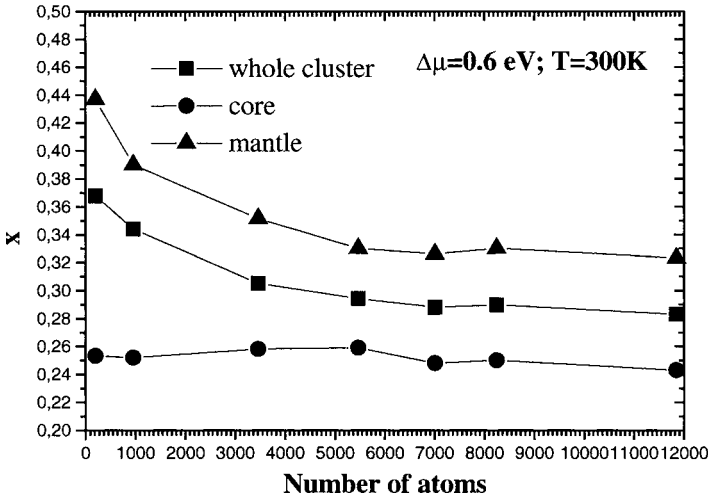

Figure 9. Calculated equilibrium concentration of Al, x, as a function of the number of the atoms in the NiAl nanocluster at zero pressure and at the same chemical potential difference of $\Delta\mu = 0.6$ eV.

there is no sharp boundary between the mantle and core regions. As already mentioned, the core radius is around 60–70% of the total cluster radius. This behaviour of the segregation is not dependent on the morphology of the cluster. As an example, figure 10(b) demonstrates the same dependence as shown in figure 10(a), in the same conditions, but for faceted 1289 atoms clusters which have the form of an ideal truncated octahedron. For the comparison, the cluster volume was subdivided into 12 layers of equal thickness, self-similar to the truncated octahedral surface. The same subdivision was made in the spherical cluster. The Al concentration among the Ni first neighbours, measured in each layer, is plotted layer by layer, each layer being self-similar to the cluster surface. For comparison, the results for the spherical 959 atom cluster are reproduced in this figure. One can see that the segregation effect in both clusters is very similar. Therefore, there is no significant influence of the morphology of the free cluster on the surface segregation.

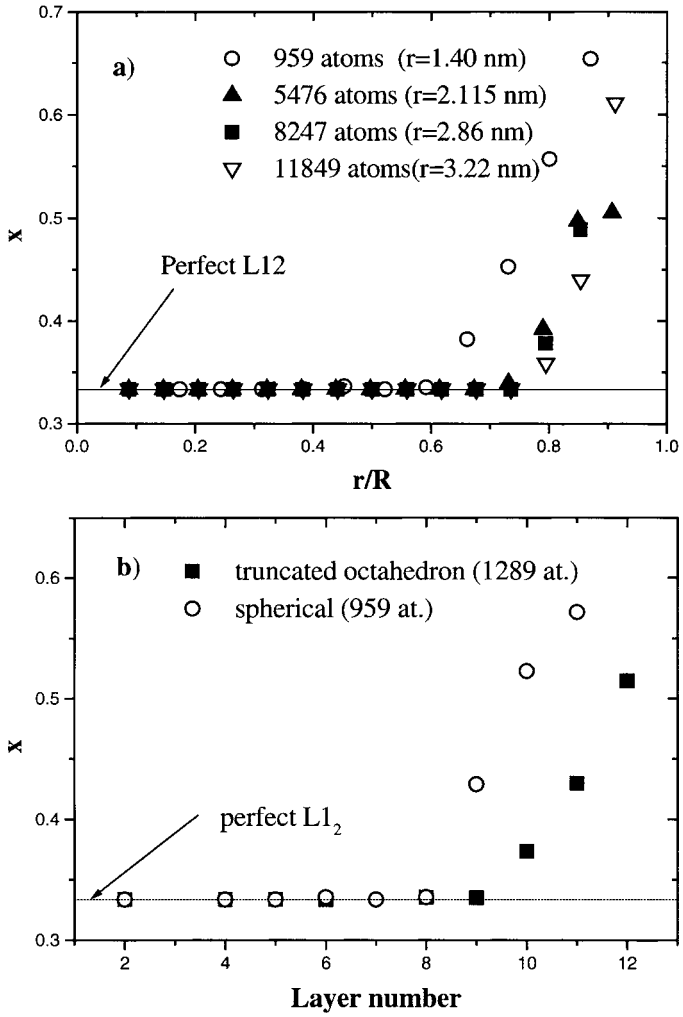

Figure 10. Concentration of Al among first neighbours of Ni as a function of the relative radial central distance for spherical clusters containing 959, 5476, 8247 and 11 849 atoms. r is the distance from the cluster centre and R is the cluster radius. (a) Spherical clusters containing 959, 5476, 8247 and 11 849 atoms. The cluster radii are indicated in the inset. (b) Spherical cluster containing 959 atoms and ideal truncated octahedron containing 1289 atoms. The chemical potential difference is 0.6 eV. Here, the Al concentration is measured in 12 equal thickness truncated octahedral layers (see text).

5. Conclusion

Before summarizing the main outcomes of the present work, a comment may be useful about the purpose of modelling. Both the MD and the MC methods used are based on the same cohesion model, namely, the second moment approximation of the tight binding model. Although this model assumes cohesion properties to scale with the filling of the d band, its success for systems where it is either empty or full is admitted, on the basis of comparison with experiment, which justified its use for copper, nickel, aluminium and their alloys. In this work, however, special care was taken to assess the model for Ni_xAl_{1-x} alloys as its empirical

parameters were initially adjusted for $x = 0.75$ only. We successfully demonstrated its ability to correctly predict the $L1_2$ and the B2 stable phases as well as the metastable character of the $L1_0$ martensitic phase.

The design of such cohesion models is useful provided they allow prediction of properties beyond those used for their assessment. This motivates the application of the second moment approximation to reduced dimensionality systems as free nanoclusters, taking care, when possible, to relate their specific properties to those of bulk materials for which they were designed.

Elemental copper is the best suited therefore since it has been the subject of many experimental and theoretical studies. This makes it possible to assess the limits of validity of the classical method employed. No such point of comparison is available for Ni–Al alloys. However, the electronic structures of Cu, Ni and Al are sufficiently close in order to suggest that elemental copper cluster properties may be compared to those of Ni–Al alloys.

A number of predictions are made. Configuration energies decrease with cluster size and are not very dependent on morphology at 0 K. This suggests the possible occurrence of isomers in free space. Cu and Ni–Al clusters are structureless if the number of atoms forming them is less than $n = 201$, corresponding to the smallest ideal fcc truncated octahedron. The only exceptions are the icosahedral structures possible for $n = 13$ and, as far as elemental clusters are concerned, also $n = 55$, 135 and 147. The bimetallic clusters have the same stable phases as the bulk material, namely $L1_2$ and B2. A distinction must be made however between the core and the surrounding disordered mantle in case of deviations from overall ideal stoichiometries. No disordered mantle is found in elemental clusters. The bimetallic core then remains stoichiometric while the mantle may be subjected to Al segregation. On the one hand, at a given chemical potential difference, aluminium segregation decreases with increasing cluster size while on the other, provided more than one thousand atoms form the cluster, the relative thickness of the mantle is not significantly size dependent. Finally, because of this partition between the ideal core and the surrounding mantle in which aluminium may accumulate, no metastable martensitic phase can be found in the core. The possible occurrence of a critical size for the austensitic/martensitic phase transition is plausible and its discussion is planned for further work.

Unfortunately, the experimental study of free clusters requires their observation 'on the fly' in order to avoid any interfacial interactions. Therefore, accessible experimental observation is rather limited. Some diffraction data for copper clusters are available, that are consistent with the present predictions. This is not sufficient however to assess the predictions listed above.

One way to overcome this limitation is to assemble clusters into nanostructured solids, which can be observed and characterized by a number of experimental techniques. Cluster assembling may well modify the cluster properties, but these modifications can be modelled at the atomic scale with techniques similar to those used in the present work. Such a programme is presently in progress, which will be the subject of further reports discussing the extent to which free cluster properties, as here predicted, remain in nanostructured materials.

Acknowledgments

It is a pleasure to acknowledge fruitful discussions with many colleagues and, in particular, with S Ramos de Debiaggi and A Caro about modelling as well as with M Yandouzi about the relation with experimental observations. One of us (EZ) is grateful to the OSTC of the Federal Belgian Government for a grant making his contribution possible during a stay at the Université Libre de Bruxelles. This research is part of a co-operative programme supported under contract PAI/IUAP 4/10 of the Federal Belgian Government.

References

[1] Giorgio S, Chapon C, Nihoul G and Penisson J M 1991 *Phil. Mag.* A **64** 87
Giorgio S, Chapon C, Henry C R and Nihoul G 1993 *Phil. Mag.* B **67** 773
Giorgio S, Graoui H, Chapon C and Henry C R 1998 *Cryst. Res. Technol.* **33** 1061
[2] Catlow C R A, Bulatov V L and Grimes R W 1997 *Nucl. Instrum. Methods* B **122** 301
[3] Hou Q, Hou M, Bardotti L, Prével B, Mélinon P and Perez A 2000 *Phys. Rev.* B at press
Bardotti L, Prével B, Mélinon P, Perez A, Hou Q and Hou M 2000 *Phys. Rev.* B at press
[4] Hou M, El Azzaoui M, Pattyn H, Verheijden J, Knoops G and Zhang G 2000 *Phys. Rev.* B at press
[5] Hohenberg P and Kohn W 1964 *Phys. Rev.* **136** 864
Kohn W and Sham L J 1965 *Phys. Rev.* **140** 1133
[6] Lammers U and Borstel G 1994 *Phys. Rev.* B **49** 17 360
[7] Massobrio C, Pasquarello A and Car R 1995 *Chem. Phys. Lett.* **238** 215
[8] Car R and Parinello M 1985 *Phys. Rev. Lett.* **55** 2471
[9] See e.g. Wales D J 1966 *Science* **271** 42
[10] Senet P and Hou M 1999 *Nanostruct. Mater.* **15** 361
[11] Schryvers D 1993 *Phil. Mag.* A **68** 1017
[12] Van Hardeveld R and Hertog F 1969 *Surf. Sci.* **15** 189
[13] Ducatselle F 1970 *J. Physique* **31** 1055
[14] Ackland G J and Vitek V 1990 *Phys. Rev.* B **41** 10 324
[15] Gao F, Bacon D and Ackland G 1993 *Phil. Mag.* A **67** 275
[16] Ackland G J and Vitek V 1989 *Mater. Res. Soc. Proc.* **133** 105
[17] Yan M and Vitek V 1995 *Interface Sci.* **3** 17
[18] El Azaoui M and Hou M 1996 *J. Phys.: Condens. Matter* **8** 6833
[19] Hou M and El Azzaoui M 1997 *Surf. Sci.* **380** 210
[20] Allen M P and Tildesley D 1987 *Computer Simulation of Liquids* (Oxford: Clarendon)
[21] Foiles S M 1985 *Phys. Rev.* B **32** 7685
[22] Chandler D 1987 *Introduction to Modern Statistical Mechanics* (New York: Oxford University Press) p 16
[23] Valkealathi S and Manninen M 1992 *Phys. Rev.* B **45** 9459
[24] Li X, Wu H, Wang X-B and Wang L-S 1998 *Phys. Rev. Lett.* **81** 1909
[25] Haberlen O D, Chung S C and Rösch N 1994 *Int. J. Quantum Chem.* **S28** 595
[26] Watari N and Ohuishi S 1998 *Phys. Rev.* B **58** 1665
[27] Kitakami O, Sato H, Shimida Y, Sato F and Tanaka M 1997 *Phys. Rev.* B **56** 13 849
[28] Reinhart D, Hall B D, Bertoud P, Valkealatahti S and Monot R 1997 *Phys. Rev. Lett.* **79** 1459
Reinhart D, Hall B D, Bertoud P, Valkealatahti S and Monot R 1998 *Phys. Rev.* B **58** 4917
[29] Muto S and Schryvers D 1993 *Acta Metall. Mater.* **41** 2377
[30] Foiles S M and Daw M S 1987 *J. Mater. Res.* **2** 5
[31] Parinello M and Rahman A 1980 *Phys. Rev. Lett.* **45** 1196
[32] Parinello M and Rahman A 1981 *J. Appl. Phys.* **52** 7182
[33] Campillo J M, Ramos de Debiaggi S and Caro A 1999 *J. Mater. Res.* **14** 2849